Journal of Applied Polymer Science

Resonance Tracking Atomic Force Acoustic Microscopy Quantitative Modulus Mapping of Carbon Nanotubes-Reinforced Acrylonitrile–Butadiene–Styrene Polymer

Flores-Ruiz Francisco Javier,[1] Reyes-Reyes José Luis,[2] Chiñas-Castillo Fernando,[2] Espinoza-Beltrán Francisco Javier[1]

[1]CINVESTAV-Querétaro, Querétaro, Qro C.P. 76230, México

[2]Department of Mechanical Engineering, Instituto Tecnológico de Oaxaca, Oaxaca, Oax C.P. 68030, México

Correspondence to: C.-C. Fernando (E-mail: fernandochinas@gmail.com)

ABSTRACT: This work presents a resonance tracking atomic force acoustic microscopy (RT-AFAM) quantitative modulus mapping of carbon nanotubes-reinforced acrylonitrile–butadiene–styrene polymer. RT-AFAM average local modulus values registered were in good agreement with those measured by nanoindentation test. RT-AFAM mapping modulus, nanoindentation, and transmission electron microscopy imaging showed that carbon nanotubes reinforcement of acrylonitrile–butadiene–styrene polymer matrix gives an elastic modulus enhancement of approximately 18.3% compared with the polymer matrix alone and showed that this technique provides high spatial resolution and helps to characterize the elastic properties of reinforced thermoplastic polymers and new compound materials at nanoscale. © 2014 Wiley Periodicals, Inc. J. Appl. Polym. Sci. **2014**, *131*, 40628.

KEYWORDS: composites; graphene and fullerenes; mechanical properties; nanotubes; synthesis and processing; thermoplastics

Received 16 December 2013; accepted 19 February 2014

DOI: 10.1002/app.40628

INTRODUCTION

Acrylonitrile–butadiene–styrene (ABS) is a copolymer widely used from musical instruments to automotive applications. In particular applications such as automotive bumper bars or protective headgears, a structural reinforcement is desirable. Carbon nanotubes (CNTs) exhibit remarkable physical properties[1] that make them ideal for several engineering applications[2] ranging from electrical conductive composites[3] to mechanically reinforced composites.[4] To incorporate CNTs into ABS polymer matrix, miscibility is a key factor, and it affects the mechanical properties of the resulting nanocomposite. A poor miscibility means poor nanocomposite reinforcement. The mixing of ABS and CNTs as a single nanocomposite material is possible when there exists a high miscibility between both materials, improving its stiffness and strength. Miscibility of the two components is generally observed by transmission electron microscopy (TEM).[3–5] For TEM measurements, sample preparation is complicated, but resolution is very good, and shape and distribution of the CNTs into the ABS polymer matrix can be observed. Mechanical properties of polymers in the nanometric scale cannot be obtained by conventional microscopy techniques; in that case, nanoindentation tests are typically used for mechanical characterization of polymers.[6,7] When fibers or CNTs are introduced as reinforcements into the polymer matrix to form a nanocomposite, the elastic modulus values registered are an average of the components that may or may not have a high dispersion. Resonance tracking atomic force acoustic microscopy (RT-AFAM)[8–10] has proven to be a sensitive technique that provides contrasted images of mechanical properties of the material being analyzed. Resolution of AFAM imaging is a function of tip radius (between 5 and 50 nm), and sample preparation does not consume much time; only a flat and smooth sample is necessary to obtain images of stiffness or elastic modulus with very high resolution, being very suitable for nanoscale characterization. The forces applied by the oscillating cantilever in contact with the sample surface usually are in the range from tens of nN (1×10–9 N) to few μN (1×10–6 N), which only cause elastic deformation of the tip–sample contact.

Previous works show that AFAM technique has been used successfully to determine elastic properties of thin films,[11,12] hard coatings,[8] piezoelectric ceramic materials,[8,11] precipitates in alloys,[13] and nanoporous materials.[14] Yamanaka et al.[15] used ultrasonic atomic force microscopy to measure carbon fiber-reinforced plastic composite, reporting only the resonance frequency shift associated with the elastic modulus for a plastic material and carbon fiber. Kos and Hurley[16] generated a

© 2014 Wiley Periodicals, Inc.

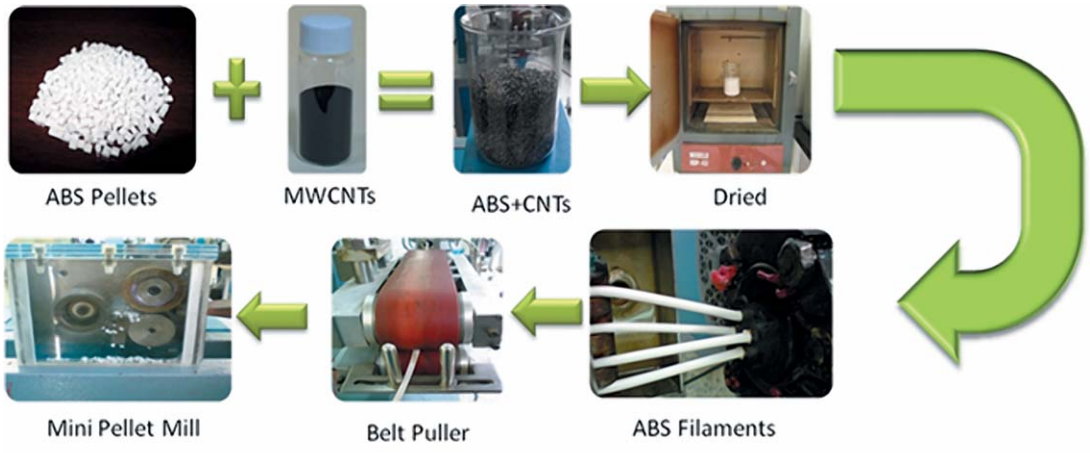

Figure 1. Extrusion process of ABS polymer and ABS + 0.5% CNTs. [Color figure can be viewed in the online issue, which is available at wileyonlinelibrary.com.]

normalized vertical contact stiffness map (k*/kc) for glass fiber–polymer matrix composite from contact resonance frequency images. Recently, Zhou et al.[17] measured an indentation modulus of glass fiber-reinforced epoxy polymer composite using AFAM. Yablon et al.[18] determined the viscoelastic properties of polyolefin blends with RT-AFAM.

As far as the authors are concerned, no work has been reported that measures the elastic properties of CNT-reinforced ABS polymer (one of the most important engineering two-phase system thermoplastics) nanocomposites using RT-AFAM. Thus, in this article, authors use an RT-AFAM mapping technique[8] to quantitatively evaluate elastic modulus properties at nanoscale resolution of CNTs-reinforced ABS polymer samples prepared by extrusion compounding–injection molding process.

EXPERIMENTAL

Polymer Nanocomposite Preparation

A medium impact, general purpose, ABS Cycolac MG47 commercial resin from Sabic Innovative Plastics US, LLC, was used for this work. CNTs used as reinforcement of the ABS polymer matrix were prepared by spray pyrolysis as described in Ref. 19 and added as prepared.

First, because ABS polymer pellets are hygroscopic, they were dried in an oven for 1 hr at 80°C (for nanocomposite making,

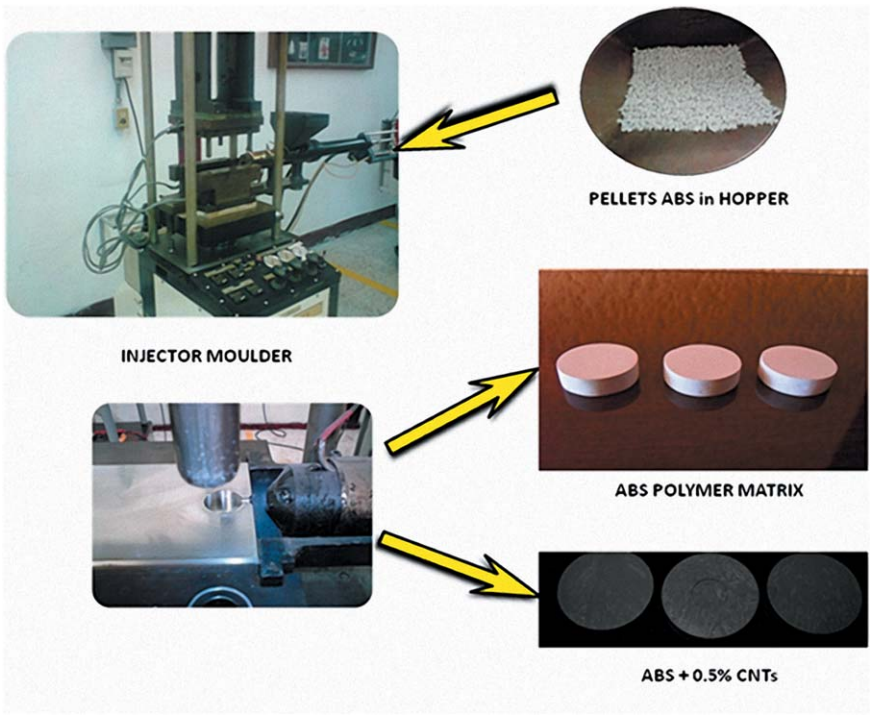

Figure 2. Injection molding process of ABS polymer and ABS + 0.5% CNTs. [Color figure can be viewed in the online issue, which is available at wileyonlinelibrary.com.]

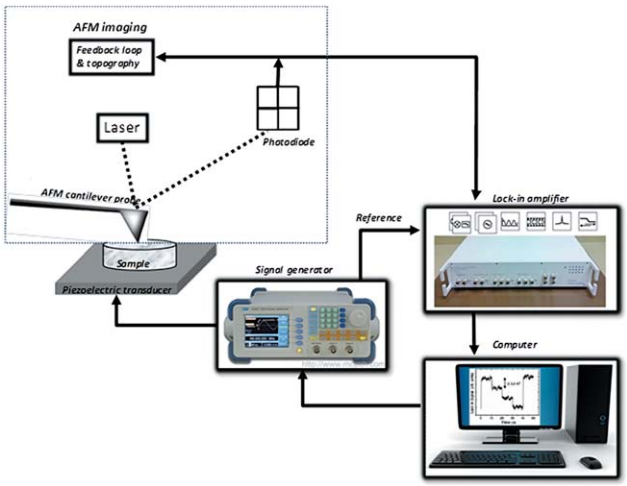

Figure 3. RT-AFAM basic principle. [Color figure can be viewed in the online issue, which is available at wileyonlinelibrary.com.]

polymer was mixed with CNTs). After that, samples of ABS polymer containing CNTs were prepared by extrusion compounding–injection molding process (Figures 1 and 2). ABS polymer material and CNT filler were mixed and fed into a mechanical single-screw extruder (Beutelspacher, Mexico) with length/diameter ratio of $L/D = 24 : 1$, for melt blending. The compounding was carried out using a screw rotation speed of 20 rpm. The temperatures setting from the hopper to the die was 174°C/100°C/165°C/160°C.

After the first pass through the single-screw extruder, the extruded strands (ABS polymer and ABS + 0.5% CNTs) of material were quenched immediately in water at room temperature and chopped into pellets by using a pelletizing machine. The obtained pellets were dried at 80°C for 1 hr in an air oven to avoid possible moisture degradation reactions prior to a second extrusion process. A highly homogenous material was obtained after the second extrusion, pelletizing, and drying process. Then, nanocomposite dried pellets went through an injection molding process using a Fox & Oxford Unimoulder U 1469 manual plastic injection molding machine with a barrel temperature profile setting ranged from 200°C to 230°C and a mold temperature kept at 40°C. Some injection parameters selected were an injection time of ABS polymer in the mold of 6 sec, an injection hold time of 10 sec, and a hydraulic contact pressure of 500 kN to finally get nanocomposite disc samples with 0.5 wt % CNTs in the ABS matrix of 25.4 mm in diameter and 10 mm thickness. As a reference, neat ABS was also similarly extruded and injection molded for this study.

Structural and Morphological Characterization

Transmission Electron Microscopy. Structure of the injection-molded CNTs-reinforced ABS nanocomposites was evaluated by TEM on an FEI TITAN 80[hyphen]300 with acceleration voltage of 300 kV. The nanocomposite specimens followed a staining with 2 wt % OsO_4 in vapour of aqueous solution for 48 hrs and then were cut using a Leica cryoultramicrotome at a sample temperature of liquid nitrogen and diamond knife temperature (−35°C) to obtain ultrathin sections with thickness approximately 70 nm and collected on a 300 mesh copper grid of 3 mm diameter. The micrographs were taken close to Scherzer defocus for an optimal contrast of the nanotubes.

Infrared Spectroscopy. Chemical analysis of the CNTs-reinforced ABS nanocomposites was performed by Fourier transform infrared (FT-IR) spectra on a Perkin–Elmer spectrophotometer using an attenuated total reflexion accessory in the 4000–650 cm^{-1} range. Resolution was set to 4 cm^{-1}, and the spectra shown were an average of 32 scans.

Nanoindentation Test. The nanoindentation technique has proven to be useful for the evaluation of mechanical properties at the nano- and microscale.[20–24] In this study, nanoindentation tests were performed using an IBIS nanoindentation system (Fisher-Cripps Laboratories), and indents were made by a three-sided pyramidal diamond Berkovich tip with nominal radius of curvature between 100 and 200 nm. Force and displacement resolution were about 0.015 μN and 0.0015 nm, respectively. At least 19 indents were performed with loads decreasing from 400 to 40 mN in steps of 20 mN on ABS polymer and ABS + 0.5% CNTs specimens, and the distance between the indentations was 80 microns to avoid plastic deformation interaction. The Berkovich tip of the nanoindenter was calibrated against a fused silica ($E = 72.5$ GPa and $H = 9.5$ GPa) and polycarbonate ($E = 3$ GPa and $H = 0.19$ GPa) standards according to Ref. 25 prior to nanoindentations on sample specimens. The peak load was held at maximum value for 60 sec to avoid the creep that would otherwise affect the unloading behavior. The Berkovich indenter was then withdrawn from the surface at the same rate until 10% of the maximum load, followed by the indenter being completely removed from the material. Here, constant strain rate was chosen to load the samples to avoid strain-hardening effects on the measurements.[26]

Principle of Modulus Mapping Using RT-AFAM

A commercial SPM-AFM system (Bruker/Veeco/Digital Instruments Nanoscope IV Dimension 3100) was used to carry out measurements of RT-AFAM on specimens made of ABS polymer and CNTs/ABS nanocomposite, using a diamond-coated silicon AFM probe (BudgetSensors model ContDLC) with nominal length of 450 μm, first resonance frequency of 13 kHz, and spring constant of 0.2 N/m.

In RT-AFAM, vibration of the probe was produced via a piezoelectric device below the sample, which was excited by a sweep AC frequency signal from a function generator. The frequency of this excitation was swept around the resonance frequency of AFM cantilever in contact with the sample. A photodiode detector followed the cantilever vibration sending a feed-back signal to a high-frequency lock-in amplifier (HF2LI, Zurich Instruments). Then this signal was amplified and filtered using the excitation signal as a reference. The amplitude spectra were fitted to a simple harmonic oscillator model for each pixel in a 256 × 256 pixels image that produce quantitative maps of maximum amplitude, phase, resonance frequency, quality factor, and topography simultaneously. Figure 3 illustrates the RT-AFAM operation principle.

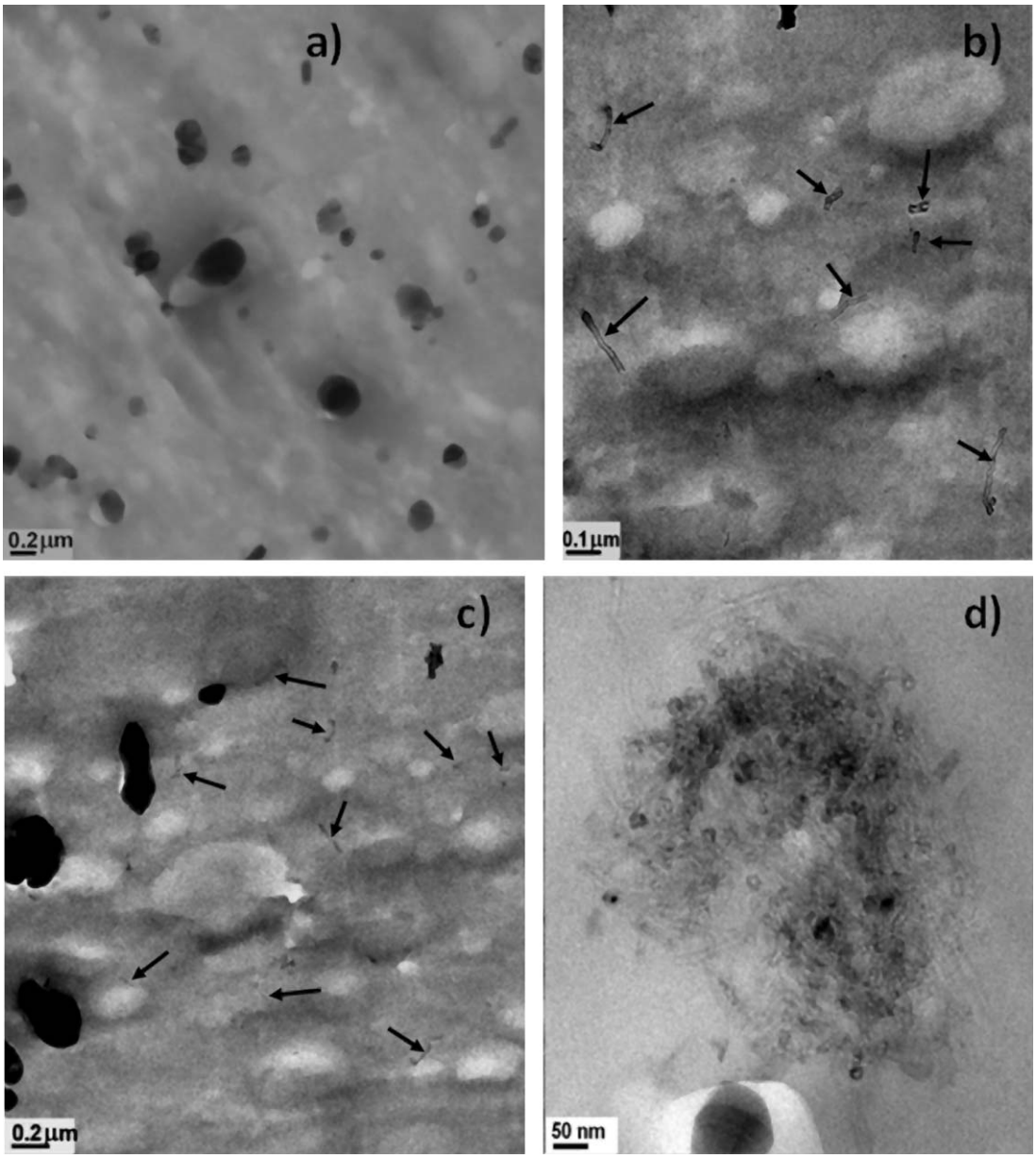

Figure 4. TEM micrographs of (a) neat ABS polymer; (b) individual CNTs in ABS polymer matrix; (c) individual CNTs in ABS polymer matrix; and (d) CNTs bundle in ABS.

RESULTS AND DISCUSSION

TEM and IR Spectroscopy

Representative TEM micrographs of specimens under study are shown in Figure 4(a–d). Figure 4(a) shows the TEM image of ABS reference specimen, indicating dark domains that represent the butadiene phase and light regions that represent acrylonitrile–styrene phase (SAN) in the ABS polymer matrix.

TEM images were taken to observe the morphology of nanocomposite samples under study in three different magnifications. Figure 4(b,c) illustrate TEM micrographs of CNTs clusters indicated by black arrows of the nanocomposite sample polymer ABS/CNTs. Figure 4(d) shows a bundle of aggregated CNTs clearly immersed in ABS polymer matrix. The size of CNT particles in Figure 4(b) is noticeably small.

Figure 5 shows the FT-IR absorbance spectra of ABS polymer matrix and CNTs-reinforced ABS nanocomposite samples. There are two bands associated to symmetric–asymmetric stretching of methylene (CH_2) in 2921 and 2851 cm^{-1} as reported in Ref. 27. Nitrile ($C{\equiv}N$) peak appears at 2238 cm^{-1} as reported in Refs. 28 and [29]. In Figure 5, no difference was observed in FT-IR absorbance spectra for the ABS + 0.5% CNT nanocomposite, but Zhuo-Yue et al.[30] reported that CNTs interact with absorbance intensity.

Figure 6 shows an intensity decay of absorbance and a slight shift in wavenumber of nitrile group in the range of 2500–2000 cm^{-1} in the FT-IR spectra for ABS + 0.5% CNT nanocomposite, suggesting some intermolecular interaction of CNTs–ABS polymer.

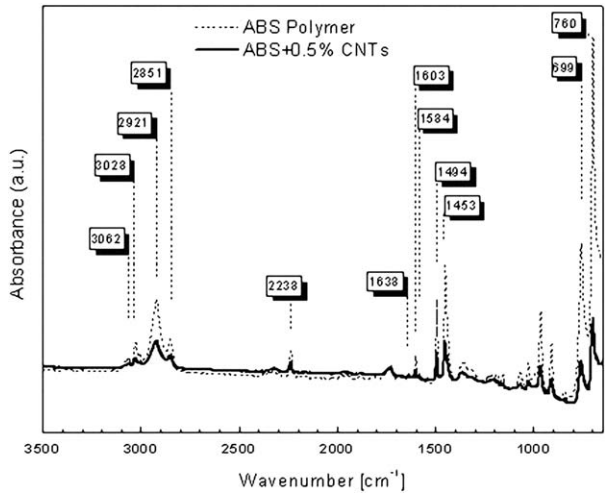

Figure 5. FT-IR absorbance spectra of ABS polymer and ABS + 0.5% CNT nanocomposite.

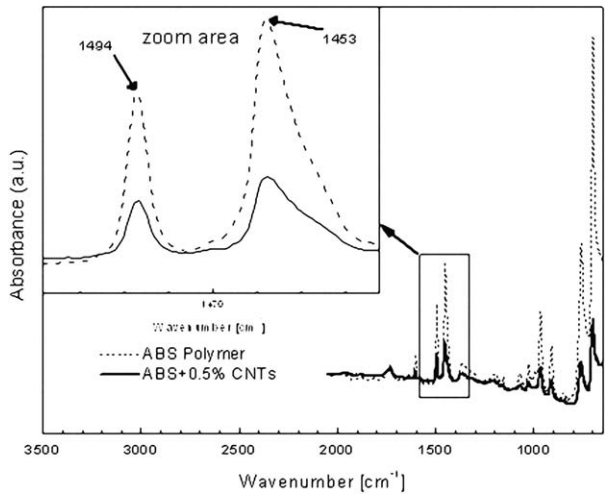

Figure 6. Zoom area of FT-IR absorbance spectra of ABS polymer and ABS + 0.5% CNT nanocomposite.

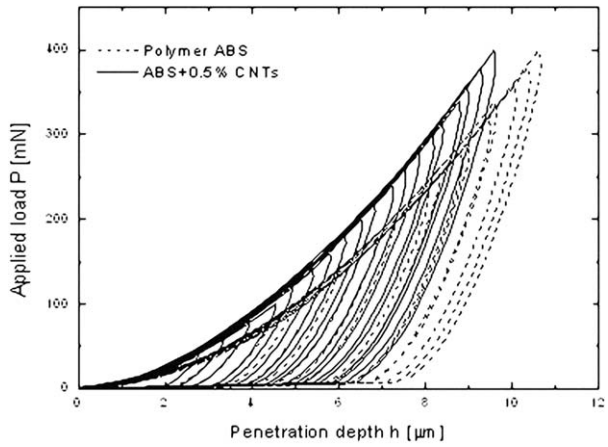

Figure 7. Nanoindentation load vs. penetration depth for ABS polymer and CNTs/ABS nanocomposite.

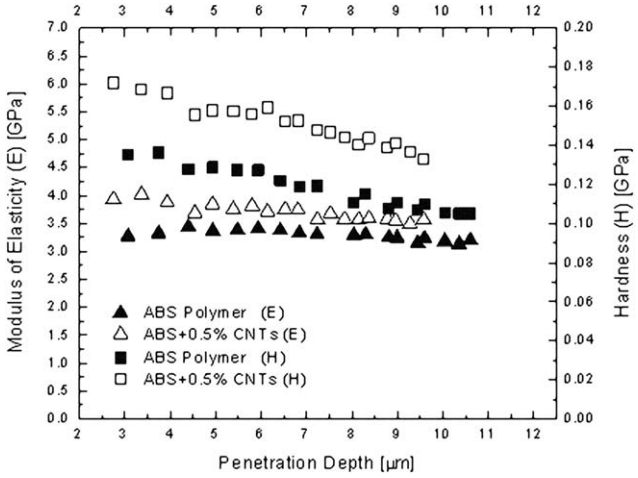

Figure 8. Elastic modulus and hardness for ABS polymer and CNTs/ABS nanocomposite.

Nanoindentation Test Results

Nanoindentation tests were carried out to obtain the aC value over the surface of the ABS polymer and CNTs/ABS nanocomposite sample. An aC radius value of 25 nm was calculated from the equation $aC=<kN>/(2E^*)$, where <kN> is the average normal stiffness of an image, and E^* is the reduced elastic modulus obtained from the nanoindentation test. Figure 7 shows nanoindentation load vs. displacement curves for both ABS polymer and CNTs/ABS nanocomposite samples using a Berkovich indenter. A shift to the left was observed in the CNTs/ABS nanocomposite load vs. displacement curve that indicated a higher elastic modulus. Nanoindentation results in Figure 8 show an average elastic modulus value of 4.0 ± 0.83 GPa for ABS + 0.5% CNTs, which was higher than that of the neat ABS polymer matrix (3.5 ± 0.15 GPa). A hardness value of 0.16 ± 0.05 GPa was measured for the ABS + 0.5% CNTs nanocomposite, whereas a lower hardness value of 0.11 ± 0.01 GPa was measured for the CNTs-free ABS polymer. This represented an enhancement of 14.3% in elastic modulus and 45.4% in hardness.

The data show approximately a constant elastic modulus; however, an intermittent variation in modulus indicates that the indenter might have encountered nanotube bundles and surrounding polymer matrix, which might have been modified by the presence of nanotubes.

AFAM Quantitative Measurement

The AFM cantilever probe used in this work is shown in a scanning electron microscopy image in Figure 9(a). This probe was modeled by finite element analysis considering the real geometry and anisotropic mechanical properties of single silicon crystal shown in Figure 9(b).[31,32]

Figure 10(a) shows the experimental resonance frequencies for free and contact modes. Experimental frequencies for free vibration f2 = 134.37 kHz, f4 = 461.60 kHz, and f5 = 764.06 kHz were used to obtain the best geometry parameters (length *L*, thickness *t*, major base width w1, and minor base width w2) indicated in Figure 9(b), and experimental frequencies for tip–

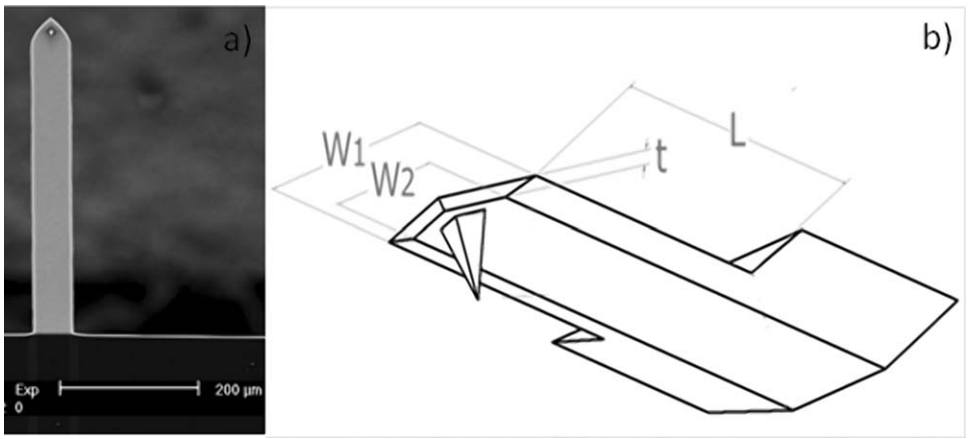

Figure 9. (a) Scanning electron microscopy micrograph of an AFM cantilever. (b) Schematic of the probe geometry used for the FEM simulations.

sample contact f3 = 405.27 kHz and f6 = 1207.03 kHz were used to simulate the contact vibration mode. Figure 10(b) shows the relation between contact resonance frequency of sixth flexural mode as a function of normal stiffness (kN). This frequency showed high sensibility with kN, which is consistent with results from Killgore and Hurley,[33] and was used to transform the map of resonance frequency into a map of normal stiffness. A reduced elastic modulus of tip–sample, E^*, was obtained from normal stiffness by using the formula $kN = 2aC E^*$, where aC is the radius of the contact area (assumed as circular) and E^* can be expressed as $1/E^* = 1/MT + 1/MS$, where MT is the indentation modulus of cantilever tip and MS is the indentation modulus of the sample.

Finite element analysis (FEA) modal analysis shown in Figure 11 gives the following results: f2 = 83.89 kHz, f3 = 235.21 kHz, f4 = 461.78 kHz, and f5 = 765.22 kHz for the free vibration mode of AFM cantilever probe. To simulate the contact, it was considered that the free end of the cantilever is anchored to three perpendicular springs, a vertical spring is related to the tip–sample normal stiffness (kN), and the two others are in plane for lateral stiffness (kS). More details about this FEA simulation can be seen in Ref. 32. Modeled frequencies for the contact vibration are f3 = 405.51 kHz and f6 = 1206.03 kHz using a kS/kN = 0.23 ratio. AFAM parameters such as spring constant (kz), geometric parameters of cantilever, and experimental and simulated resonance frequencies of the AFM cantilever are indicated in Table I.

Elastic Modulus Mapping

When a reinforcement material like CNT with high elastic modulus and chemical compatibility is introduced into a polymeric matrix, this material modifies the structure of the polymer and consequently its final mechanical properties. The polymer ABS consists of butadiene dispersed in SAN matrix.[3] Figure 12(a,b) are topography images of ABS polymer and CNTs/ABS nanocomposite samples obtained simultaneously during the RT-AFAM experiment. These images show differences in height about 100 nm for the ABS polymer sample and 60 nm for the CNTs/ABS nanocomposite sample.

Figure 13(a,b) shows the indentation modulus mapping for ABS and ABS + 0.5% CNT, respectively. It can be seen in histograms of Figure 14(a,b) that the incorporation of CNTs in the polymer matrix modifies the mechanical properties. A fitting that considers Gaussian contributions gives values of indentation modulus of 3.38 ± 0.25 GPa for ABS polymer and 4.0 ± 0.30 GPa for ABS + 0.5% CNT nanocomposite. Comparison of histograms in Figure 15 shows a shift of almost 0.62 GPa between ABS polymer and ABS + 0.5% CNT nanocomposite, which in practical terms, means an increase in the elastic modulus of 18.3%.

Figure 16(a,b) shows phase images for ABS and ABS + 0.5% CNT, where the contrast change is related to a shift of contact resonance frequency during the RT-AFAM experiment and therefore it allows observing changes in stiffness of ABS and ABS + 0.5% CNT specimens. Figure 16(a) shows the ABS polymer with three zones. The first corresponds to SAN matrix located in the range of −60° to −80°. The second zone in the range of 20°–60° is related to butadiene. The third zone corresponds to a butadiene–SAN blend between −30° and 0°. The incorporation of CNTs into the ABS polymer matrix brings an improvement in the miscibility of nanocomposite sample as illustrated in Figure 16(b) providing a more homogenous dispersion of the CNTs in the ABS polymer matrix. This effect has been explained as a double percolation phenomenon.[4]

In such a case, a load applied to the nanotubes network is more efficient and provides a more uniform stress distribution in the CNTs-reinforced ABS polymer matrix.[1] The random distribution of CNTs observed in this micrograph gives isotropic nanomechanical properties as observed in the modulus mapping for ABS/CNT nanocomposite sample shown in Figure 13(b). Figure 16(b) shows that the external stresses applied to the composite are efficiently transferred to the nanotubes and represented as minimization of abrupt changes at the interface.

At atomic scale, the elastic modulus represents the stiffness of chemical bonds. The stiffness of these bonds will depend on how the electrons of the atoms interact (i.e., whether the atoms involved are able to form crystalline or amorphous structures). At nanometric scale, the elastic modulus statistically reflects

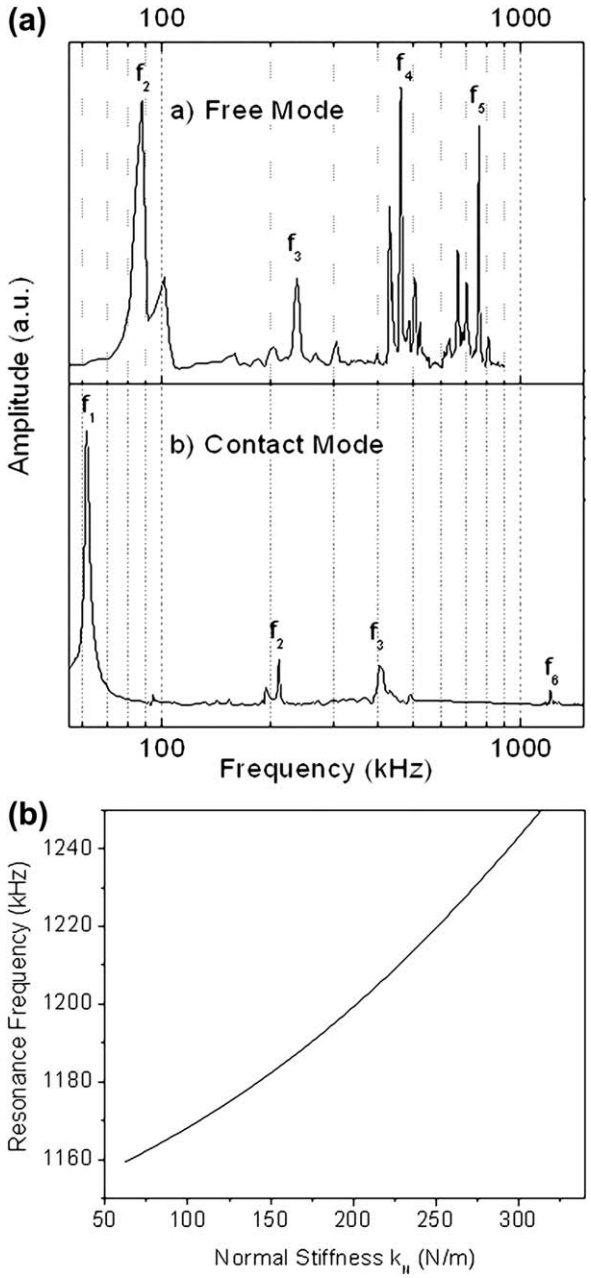

Figure 10. (a) Experimental resonance frequencies for free and contact mode. (b) Resonance frequency vs. normal stiffness.

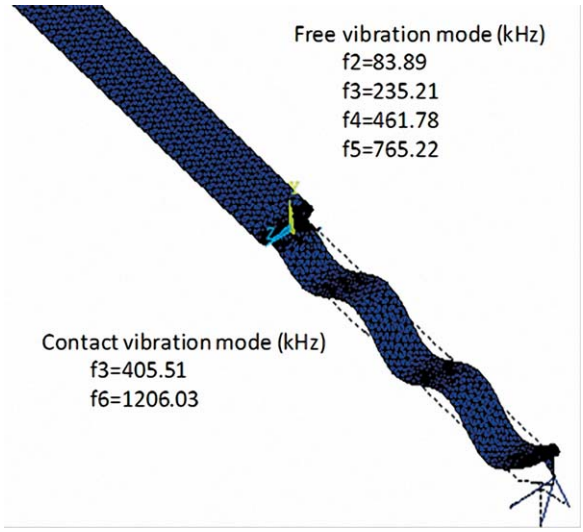

Figure 11. FEA modal analysis of AFM cantilever probe. [Color figure can be viewed in the online issue, which is available at wileyonlinelibrary.com.]

how the atoms are interacting, whereas at macroscale, the elastic modulus is dominated by the component with higher volume fraction, and the values measured were an average of the local elastic properties of the components that form the material (here imperfections in the materials also contribute to this average). In this research, the CNTs added to the ABS matrix helped to increase the elastic modulus and hardness of the composite.

CONCLUSIONS

AFAM indentation modulus mapping at nanoscale was carried out on ABS polymer and ABS + 0.5% CNT nanocomposite specimens. A complete characterization of specimens by TEM, FT-IR spectroscopy, nanoindentation tests, and FEA of the AFM probe for AFAM quantitative maps of indentation modulus were presented in this work. AFAM values of indentation modulus (ABS = 3.38 GPa and ABS + 0.5% CNT = 4.0 GPa) were in good agreement with those calculated by nanoindentation test (ABS = 3.5 GPa and ABS + 0.5% CNT = 4.0 GPa). AFAM phase images and indentation modulus mapping also show that the interfacial interaction between CNTs and polymer matrix is continuous, which gives a more uniform stress distribution and an improvement of 18.3% in elastic modulus of the nanocomposite sample.

Table I. Experimental Resonance Frequencies for Free and Contact Mode and Probe Geometry

Free resonance frequency (kHz)		Contact resonance frequency (kHz)		Spring constant (N/m)			
Exp	Simulated	Exp	Simulated			Geometry parameters (μm)	
84.37	83.89	13.37	13.37	kx	2.64	Length	465.50
234.00	235.21	210.93	208.88	ky	36.49	Major base width	59.71
461.60	461.78	405.27	405.51	kz	0.17	Minor base width	44.99
764.06	765.22	1207.03	1206.03			Thickness	2.02

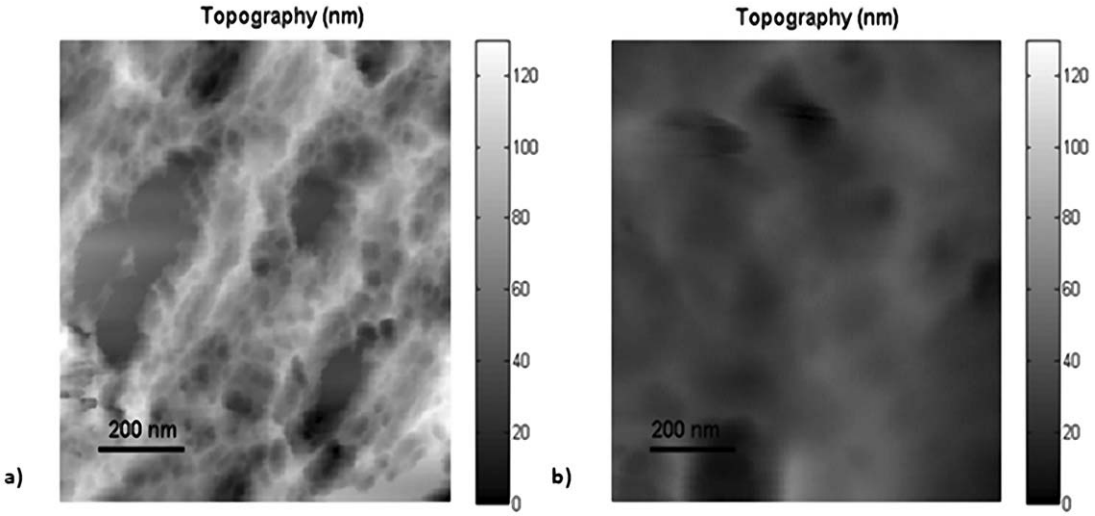

Figure 12. Topography of (a) ABS polymer and (b) CNTs/ABS nanocomposite.

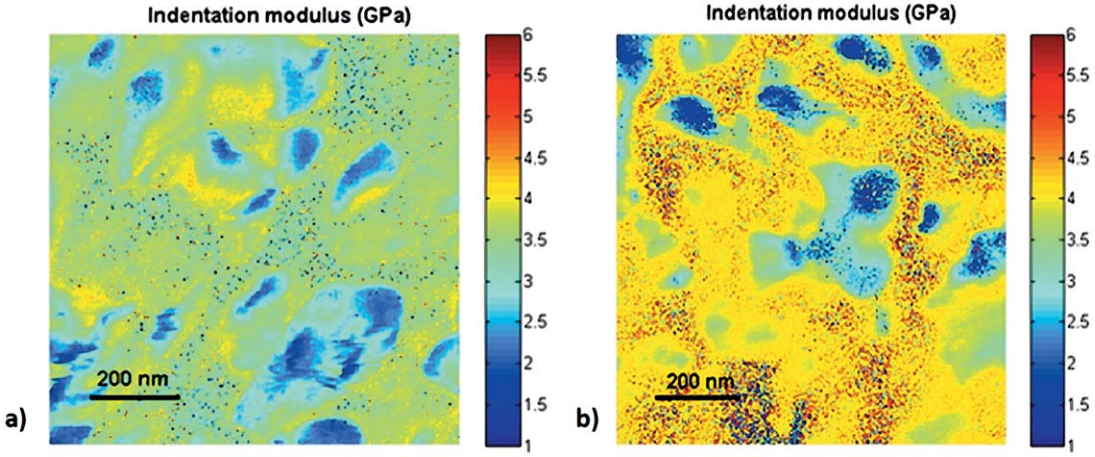

Figure 13. Indentation modulus of (a) ABS polymer and (b) CNTs/ABS nanocomposite. [Color figure can be viewed in the online issue, which is available at wileyonlinelibrary.com.]

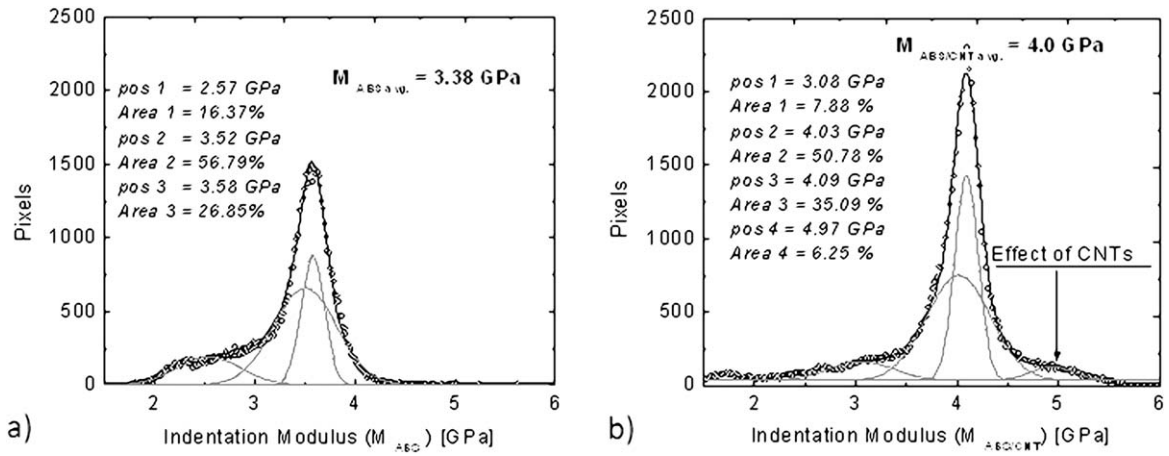

Figure 14. Histogram of (a) ABS polymer and (b) ABS/CNT nanocomposite.

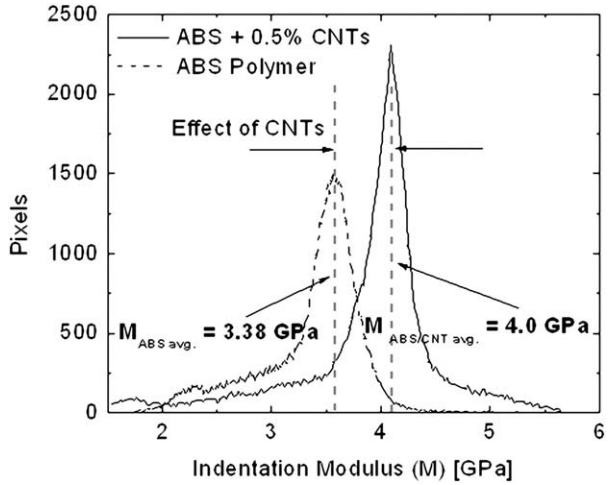

Figure 15. Comparison of RT-AFAM indentation modulus of ABS polymer and ABS/CNT nanocomposite.

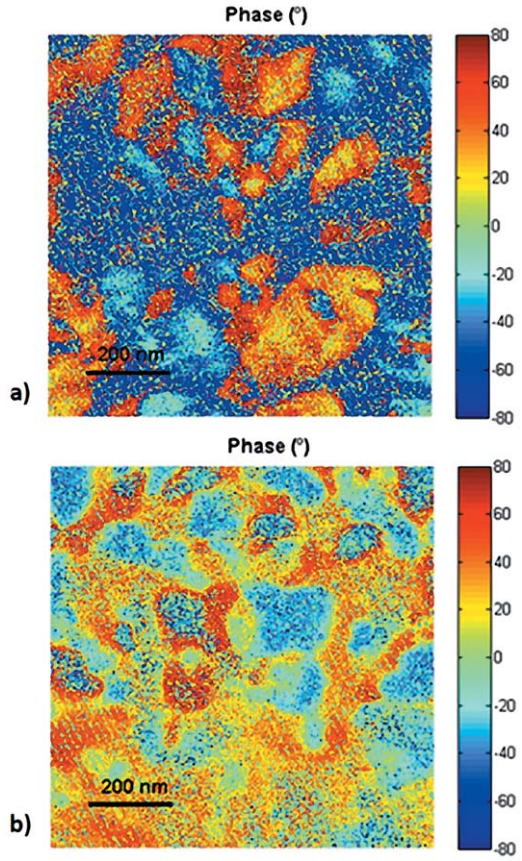

Figure 16. Phase images of (a) ABS polymer and (b) ABS/CNT nanocomposite. [Color figure can be viewed in the online issue, which is available at wileyonlinelibrary.com.]

ACKNOWLEDGMENTS

The authors thank the National Council for Science and Technology (CONACyT) and the Secretary of Public Education (SEP) for the financial support under projects 079901 to carry out the present work.

REFERENCES

1. Coleman, J. N.; Khan, U.; Gun'ko, Y. K. *Adv. Mater.* **2006**, *18*, 689.
2. Ajayan, P. M.; Zhou, O. Z. In Applications of Carbon Nanotubes; Dresselhaus, M. S., Dresselhaus, G., Avouris, P., Eds.; Springer Verlag: New York, **2001**; Vol. 80, pp 391–425.
3. Al-Saleh, M. H.; Sundararaj, U. *J. Polym. Sci. B Polym. Phys.* **2012**, *50*, 1356.
4. Meincke, O.; Kaempfer, D.; Weickmann, H.; Friedrich, Ch.; Vathauerb, M.; Warth, H. *Polymer* **2004**, *45*, 739.
5. Bhagwan, F. J.; Mayur, S.; Madan, K.; Prakash, K. B. *J. Encapsulation Adsorpt. Sci.* **2012**, *2*, 69.
6. Briscoe, B. J.; Fiori, L.; Pelillo, E. *J. Phys. D: Appl. Phys.* **1998**, *31*, 2395.
7. Cadek, M.; Coleman, J. N.; Barron, V.; Hedicke, K.; Blau, W. J. *Appl. Phys. Lett.* **2002**, *81*, 5123.
8. Enriquez-Flores, C. I.; Gervacio-Arciniega, J. J.; Cruz-Valeriano, E.; Urquijo-Ventura, P.; Gutierrez-Salazar, B. J.; Espinoza-Beltran, F. J. *Nanotechnology* **2012**, *23*, 495705.
9. Jesse, S.; Kalinin, S. V.; Proksch, R.; Baddorf, A. P.; Rodriguez, B. J. *Nanotechnology* **2007**, *18*, 435503.
10. Rodriguez, B. J.; Callahan, C.; Kalinin, S. V.; Proksch, R. *Nanotechnology* **2007**, *18*, 475504.
11. Rabe, U.; Amelio, S.; Kester, E.; Scherer, V.; Hirsekorn, S.; Arnold, W. *Ultrasonics* **2000**, *38*, 430.
12. Kopycinska-Muller, M.; Striegler, A.; Kohler, B.; Wolter, K. J. *Adv. Eng. Mater.* **2011**, *13*, 312.
13. Kumar, A.; Rabe, U.; Hirsekorn, S.; Walter, A. *Appl. Phys. Lett.* **2008**, *92*, 183106.
14. Kopycinska-Muller, M.; Yeap, K. B.; Mahajan, S.; Kohler, B.; Kuzeyeva, N.; Muller, T.; Zschech, E.; Wolter, K. J. *Nanotechnology* **2013**, *24*, 355703.
15. Yamanaka, K.; Maruyama, Y.; Tsuji, T. *Appl. Phys. Lett.* **2001**, *78*, 1939.
16. Kos, A. B.; Hurley, D. C. *Meas. Sci. Technol.* **2008**, *19*, 015504.
17. Zhou, X.; Fu, J.; Li, Y.; Li, F. *J. Appl. Polym. Sci.* **2014**, *131*, DOI: 10.1002/APP.39800.
18. Yablon, D. G.; Gannepalli, A.; Proksch, R.; Killgore, J.; Hurley, D. C.; Grabowski, J.; Tsou, A. H. *Macromolecules* **2012**, *45*, 4363.
19. Robles-Nuñez, J.; Chiñas-Castillo, F.; Sanchez-Rubio, M.; Lara-Romero, J.; Huirache-Acuña, R.; Jimenez-Sandoval, S.; Alonso-Nuñez, G. *Chem. Papers* **2012**, *66*, 1130.
20. Dutta, A. K.; Penumadu, D.; Files, B. *J. Mater. Res.* **2004**, *19*, 158.
21. Li, X.; Gao, H.; Scrivens, W. A.; Fei, D.; Xu, X.; Sutton, M. A.; Reynolds, A. P.; Myrick, M. L. *Nanotechnology* **2004**, *15*, 1416.
22. Oliver, W. C.; Pharr, G. M. *J. Mater. Res.* **1992**, *7*, 1564.
23. Oliver, W. C.; Pharr, G. M. *J. Mater. Res.* **2004**, *19*, 3.
24. Fischer-Cripps, A. C. Nanoindentation; Springer: New York, **2002**.

25. Alvarado-Orozco, J. M.; Cárdenas-Jaramillo, C.; Torres-Torres, D.; Herrera-Basurto, R.; Hurtado-Macias, A.; Muñoz-Saldaña, J.; Trápaga-Martinez, G. *Mater. Res. Soc. Symp. Proc.* **2010**, *1243*, 18.

26. Beake, B. D.; Chen, S.; Hull, J. B.; Gao, F. *J. Nanosci. Nanotechnol.* **2002**, *2*, 73.

27. He, X. J.; Wang, L. J.; Xie, X. L.; Zhang, K. *Plast. Rubber Compos.* **2010**, *39*, 54.

28. Santana-Pérez, O. Fracturas de Mezclas de Policarbonato con Acrilonitrilo-Butadieno-Estireno, Ph.D. Thesis; Universidad de Politécnica de Catalunya (UPC): Barcelona, Spain, **1997**.

29. Henniker, J. C. Infrared Spectrometry of Industrial Polymers; Academic Press: London, **1969**.

30. Zhuo-Yue, X.; Li, W.; Yao, S.; Zhao-Xia, G.; Jian, Y. *Polymer* **2013**, *54*, 447.

31. Espinoza Beltrán, F. J.; Muñoz-Saldaña, J.; Torres-Torres, D.; Torres-Martínez, R.; Schneider, G. A. *J. Mater. Res.* **2006**, *21*, 3072.

32. Espinoza-Beltrán, F. J.; Geng, K.; Muñoz-Saldaña, J.; Rabe, U.; Hirsekorn, S.; Arnold, W. *New J. Phys.* **2009**, *11*, 033034.

33. Killgore, J. P.; Hurley, D. C. *Nanotechnology* **2012**, *23*, 055702.